JOURNAL OF CLIMATE

Supplementary Tables and Figures for *"The MERRA-2 Aerosol Reanalysis, 1980 – onward, Part I: System Description and Data Assimilation Evaluation"*

C. A. RANDLES *[a]† A. M. DA SILVA [a], V. BUCHARD[a,b], P. R. COLARCO[c], A. DARMENOV[a], R. GOVINDARAJU[a,d], A. SMIRNOV[d,e], B. HOLBEN[e], R. FERRARE[f], J. HAIR[f], Y. SHINOZUKA[g,h] AND C. J. FLYNN[i]

[a]*Global Modeling and Assimilation Office, NASA Goddard Space Flight Center, Greenbelt, Maryland, USA*
[b]*GESTAR/Universities Space Research Association, Columbia, Maryland, USA*
[c]*Atmospheric Chemistry and Dynamics Lab, NASA Goddard Space Flight Center, Greenbelt, Maryland, USA*
[d]*Science Systems and Applications, Inc., Lanham, MD, USA*
[e]*NASA Biospheric Sciences Laboratory, Greenbelt, Maryland, USA*
[f]*NASA Langley Research Center, Hampton, VA, USA*
[g]*Bay Area Environmental Research Institute, Petaluma, California, USA*
[h]*NASA Ames Research Center Cooperative for Research in Earth Science and Technology, Moffett Field, California, USA*
[i]*Pacific Northwest National Laboratory, Richland, Washington, USA*

ABSTRACT

Supplementary tables and figures for *The MERRA-2 Aerosol Reanalysis, 1980 – onward, Part I: System Description and Data Assimilation Evaluation*. Table 1 shows the aerosol optical properties assumed in the Goddard Chemistry, Aerosol, Radiation, and Transport (GOCART) aerosol module as a function of aerosol species and relative humidity at 550 nm. Table 2 gives the observation error (standard deviation) and scalar Kalman gain for each aerosol sensor assimilated in the Goddard Aerosol Assimilation System (GAAS). Table 3, based on Figure 13 in the main text, compares AOD, AAOD and the shortwave, clear-sky aerosol Direct Radiative Effect (DRE) between reanalyses, models, and observations over land and ocean. Figures 1-3 show the same information as Figure 5 in the main text, but for different sensors in the aerosol observing system. Figure 4 shows probability distribution functions of observation minus forecast ($O-F$) and observation minus analysis ($O-A$) for each sensor in the aerosol observing system. Finally, the remaining figures show timeseries of AOD at various AERONET sites from Table 3 in the main text.

*Corresponding author address: C. A. Randles, 1545 US-22, Clinton, NJ, 08801
E-mail: cynema@alum.mit.edu

†now at ExxonMobil Research and Engineering

TABLE 1. Aerosol optical properties by species at $\lambda = 0.55\ \mu$m and as a function of relative humidity (RH).[a]

	Mass Extinction Coefficient[e] (β_{ext}) [m^2 g^{-1}]			Single Scattering Albedo[f] (ω_o)			Asymmetry Parameter[g] (g)		
Species	RH = 0%	RH = 80%	RH = 95%	RH = 0%	RH = 80%	RH = 95%	RH = 0%	RH = 80%	RH = 95%
Dust Bin 1[b]	2.02	2.02	2.02	0.96	0.96	0.96	0.71	0.71	0.71
Dust Bin 2[b]	0.64	0.64	0.64	0.92	0.92	0.92	0.75	0.75	0.75
Dust Bin 3[b]	0.33	0.33	0.33	0.89	0.89	0.89	0.80	0.80	0.80
Dust Bin 4[b]	0.17	0.17	0.17	0.83	0.83	0.83	0.84	0.84	0.84
Dust Bin 5[b]	0.08	0.08	0.08	0.77	0.77	0.77	0.87	0.87	0.87
Sea Salt Bin 1[c]	0.73	4.54	25.98	1.00	1.00	1.00	0.20	0.50	0.69
Sea Salt Bin 2[c]	3.48	10.01	24.02	1.00	1.00	1.00	0.70	0.78	0.79
Sea Salt Bin 3[c]	0.74	2.04	4.85	1.00	1.00	1.00	0.71	0.78	0.83
Sea Salt Bin 4[c]	0.30	0.86	2.02	1.00	1.00	1.00	0.77	0.83	0.85
Sea Salt Bin 5[c]	0.10	0.30	0.72	1.00	1.00	1.00	0.81	0.86	0.87
Hydrophobic BC[d]	9.28	9.28	9.28	0.21	0.21	0.21	0.33	0.33	0.33
Hydrophilic BC[d]	9.28	11.27	15.77	0.21	0.25	0.38	0.33	0.40	0.50
Hydrophobic OC[d]	2.67	2.67	2.67	0.96	0.96	0.96	0.58	0.58	0.58
Hydrophilic OC[d]	2.67	7.01	16.04	0.96	0.98	0.99	0.58	0.68	0.74
Sulfate[d]	3.15	14.29	22.53	1.00	1.00	1.00	0.67	0.78	0.80

[a] Optical properties are given at 0%, 80% and 95% RH for hydrophilic species; for hydrophobic species optical properties do not vary with model RH.

[b] The dry (RH = 0%) effective radii (r_{eff}) for the 5 dust bins are 0.64, 1.34, 2.32, 4.20, and 7.75 μm, respectively.

[c] The dry effective radii for the 5 sea salt bins are 0.08, 0.27, 1.05, 2.50, and 7.48, μm, respectively.

[d] The effective radii for dry sulfate, organic carbon, and black carbon are 0.16, 0.09, 0.04 μm, respectively.

[e] Mass extinction coefficient (β_{ext}) is the sum of scattering and absorption coefficients ($\beta_{ext} = \beta_{sca} + \beta_{abs}$)

[f] Single scattering albedo $\omega_o = \beta_{sca}/\beta_{ext}$; range 0 – 1 for purely absorbing to purely scattering aerosol, respectively.

[g] The asymmetry parameter g; range -1 to 1 for completely backscattering to completely forward scattering, respectively. Isotropic scattering is $g = 0$.

TABLE 2. Observation error standard deviations ($\sum^o$) and scalar Kalman gain (K) – the ratio of the background error variances and the innovation error variances – used in the PSAS-based analysis of the log-transform AOD η. For reference, the background error decorrelation length scale is 140 km, and the background error standard deviation is 0.45. Homogeneous and isotropic covariance models are assumed, with spatially constant variances. Error covariance model parameters were estimated using maximum-likelihood method of Dee and da Silva (1999).

Sensor	$\sum^o$	K
AERONET	0.20	0.84
AVHRR (Ocean)	0.20	0.84
MISR	0.15	0.90
MODIS Terra (Land)	0.20	0.84
MODIS Terra (Ocean)	0.18	0.86
MODIS Aqua (Land)	0.20	0.84
MODIS Aqua (Ocean)	0.18	0.86

TABLE 3. Clear-sky AOD, AAOD, and Direct Radiative Effect (DRE; W m^{-2}) from Reanalyses, Models, and Observations

	Yu et al. (2006) Obs.[a]	Yu et al. (2006) Models[b]	MERRA-2[c]	MERRAero[c]	MACC[d]
			Land-area Average		
AOD	0.225 ± 0.038	0.178 ± 0.029	**0.180** ± 0.027	0.171 ± 0.030	0.203 ± 0.030
AAOD	–	–	**0.012** ± 0.002	0.016 ± 0.003	0.010 ± 0.003
TOA DRE	-4.85 ± 0.45	-2.80 ± 1.19	**-3.09** ± 0.62	-3.11 ± 0.70	-6.40 ± 1.00
SFC DRE	-11.70 ±1.20	-7.20 ± 1.86	**-8.35** ± 1.82	-8.64 ± 2.04	-11.50 ± 1.90
ATM DRE	6.85 ± 0.75	4.90 ± 0.81	**5.26** ± 1.23	5.53 ± 1.37	5.10
TOA DRE Efficiency[e]	-21.56	-15.73	**-17.17**	-18.19	-31.53
			Ocean-area Average		
AOD	0.138 ± 0.024	0.100 ± 0.042	**0.123** ± 0.008	0.111 ± 0.010	0.170 ± 0.030
AAOD	–	–	**0.005** ± 0.001	0.005 ± 0.001	0.007 ± 0.001
TOA DRE	-5.45 ± 0.70	-3.50 ± 1.28	**-3.65** ± 0.21	-3.44 ± 0.24	-7.70 ± 1.50
SFC DRE	-8.80 ± 1.65	-4.80 ± 1.60	**-5.74** ± 0.41	-5.58 ± 0.47	-10.60 ± 1.90
ATM DRE	3.60 ± 1.30	1.30 ± 0.72	**2.09** ± 0.27	2.14 ± 0.29	2.90
TOA DRE Efficiency[e]	-39.49	-35.00	**-29.67**	-30.99	-45.29

[a]Median and standard deviation from satellite-derived estimates (Yu et al. 2006).

[b]Median and standard deviation from 4 global models in Yu et al. (2006).

[c]Climatological global area-weighted average (± monthly standard deviation) for Y2003-Y2010.

[d]For MACC, the Y2003-Y2010 global mean and uncertainty is given following Bellouin et al. (2013).

[e]TOA DRE Efficiency = TOA DRE/AOD

References

Bellouin, N., J. Quaas, J.-J. Morcrette, and O. Boucher, 2013: Estimates of aerosol radiative forcing from the MACC reanalysis. *Atmospheric Chemistry and Physics*, **13 (4)**, 2045–2062, doi:10.5194/acp-13-2045-2013.

Dee, D. P., and A. M. da Silva, 1999: Maximum-likelihood estimation of forecast and observation error covariance parameters. Part I: Methodology. *Monthly Weather Review*, **127**, 1811–1834.

Yu, H., and Coauthors, 2006: A review of measurement-based assessments of the aerosol direct radiative effect and forcing. *Atmospheric Chemistry and Physics*, **6 (3)**, 613–666, doi:10.5194/acp-6-613-2006.

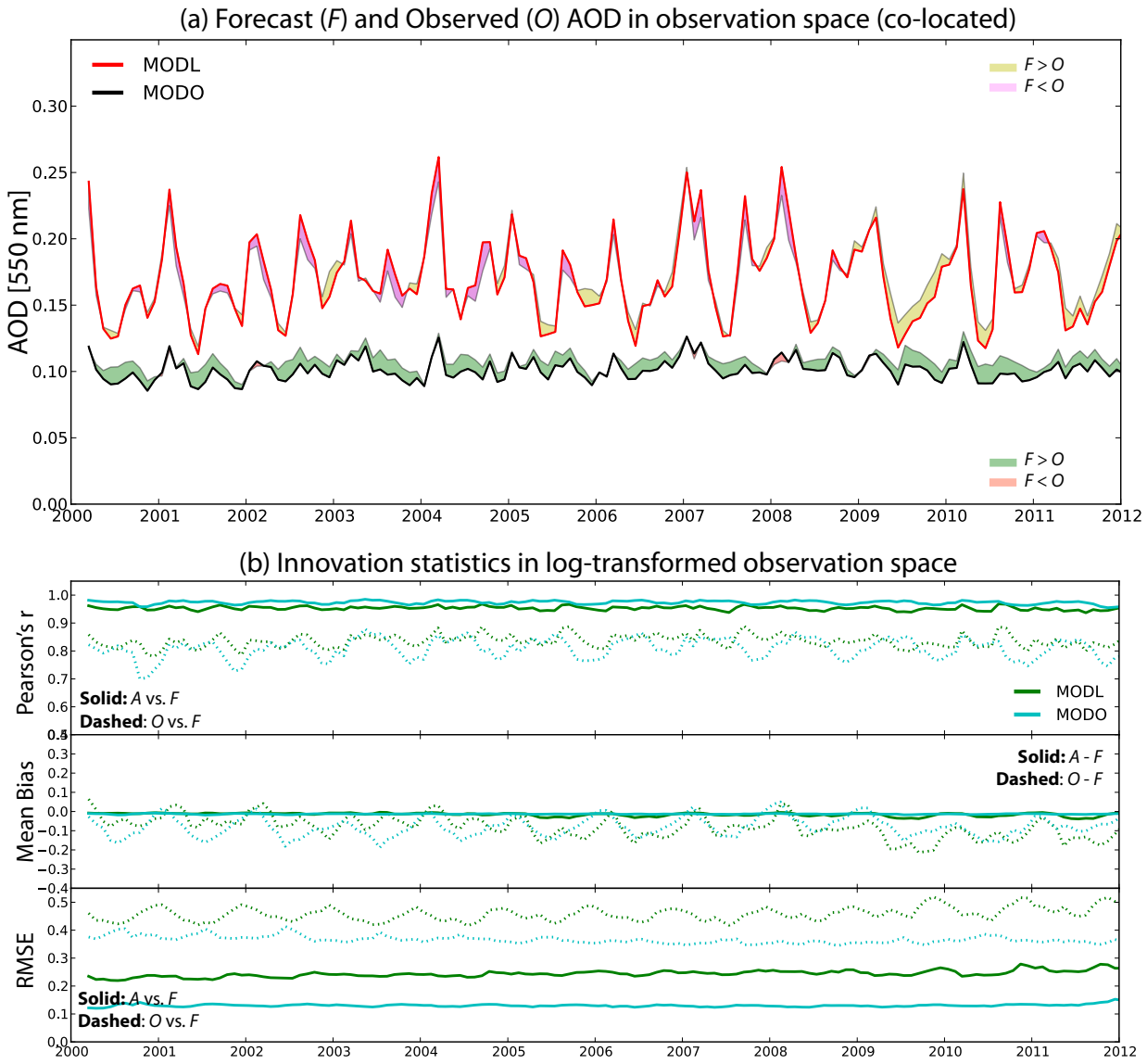

FIG. 1. (a) Co-located (pair-wise in observation space) comparison of the 3-hour model forecast (F) and observations (O) for MODIS Terra land NNR (MODL) and MODIS Terra ocean NNR (MODO). Here the lines represent the observed AOD, and shading indicates the difference between F and O. (b) Innovation statistics computed in log-transformed observation space ($ln(AOD+0.01)$). Statistics comparing O and F are shown as dashed lines, and relationships between the observations and analysis (A) are shown as solid lines for the same sensors as in (a).

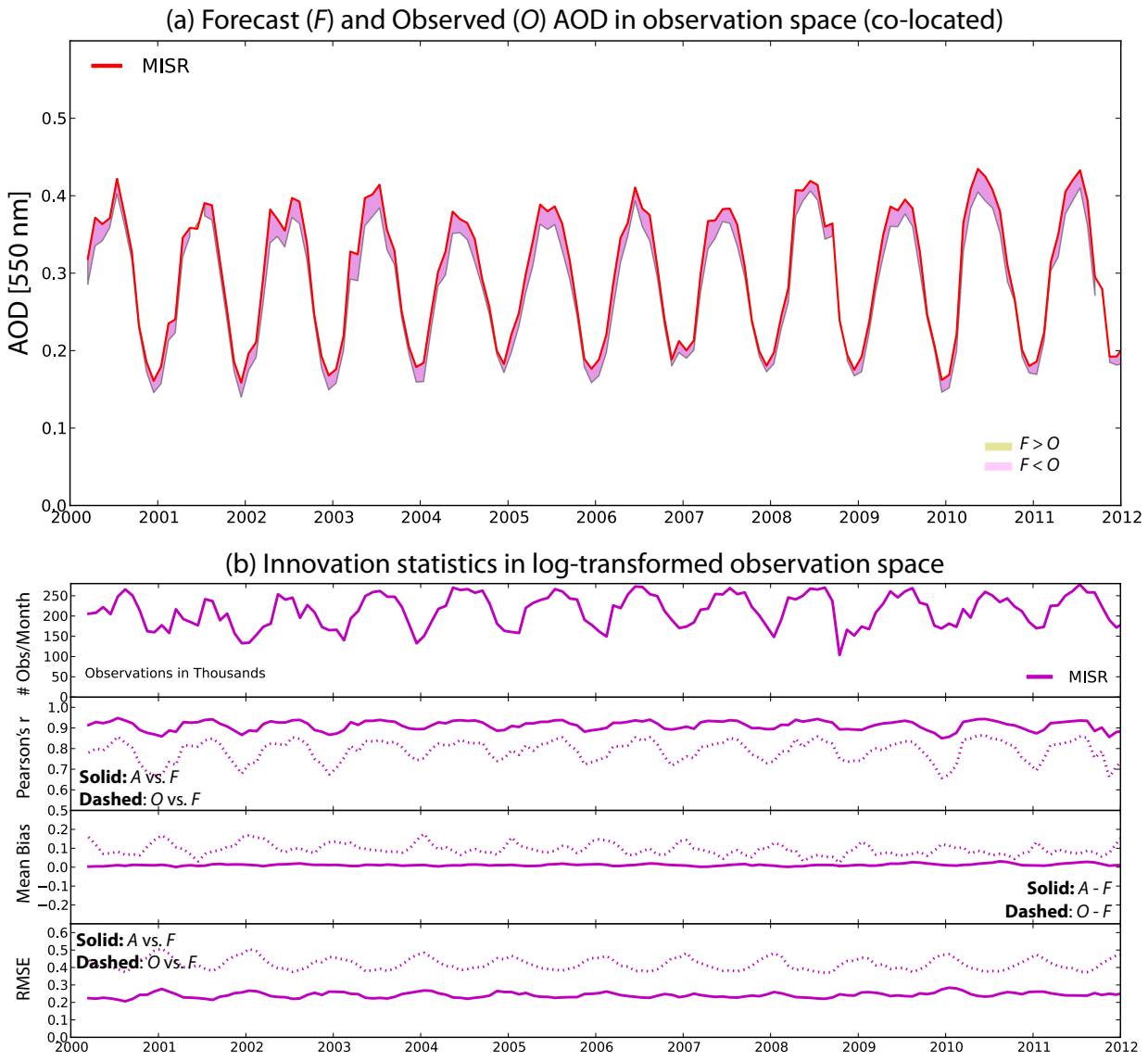

FIG. 2. (a) Co-located (pair-wise in observation space) comparison of the 3-hour model forecast (F) and observations (O) for MISR (bright surfaces only). Here the lines represent the observed AOD, and shading indicates the difference between F and O. (b) Innovation statistics computed in log-transformed observation space ($ln(AOD + 0.01)$). Statistics comparing O and F are shown as dashed lines, and relationships between the observations and analysis (A) are shown as solid lines for the same sensor as in (a).

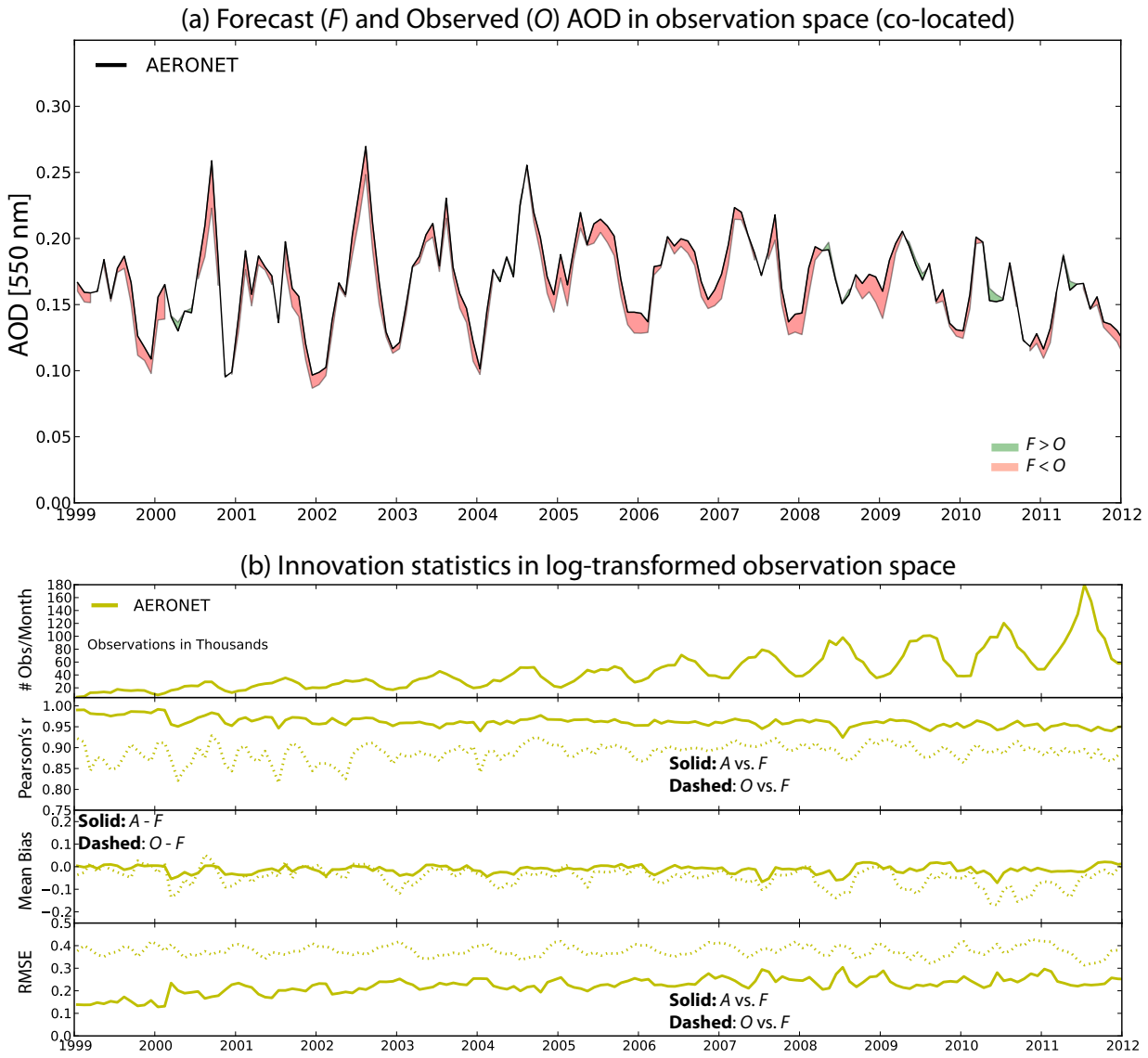

FIG. 3. (a) Co-located (pair-wise in observation space) comparison of the 3-hour model forecast (F) and observations (O) for AERONET. Here the lines represent the observed AOD, and shading indicates the difference between F and O. (b) Innovation statistics computed in log-transformed observation space ($ln(AOD + 0.01)$). Statistics comparing O and F are shown as dashed lines, and relationships between the observations and analysis (A) are shown as solid lines for the same sensor as in (a).

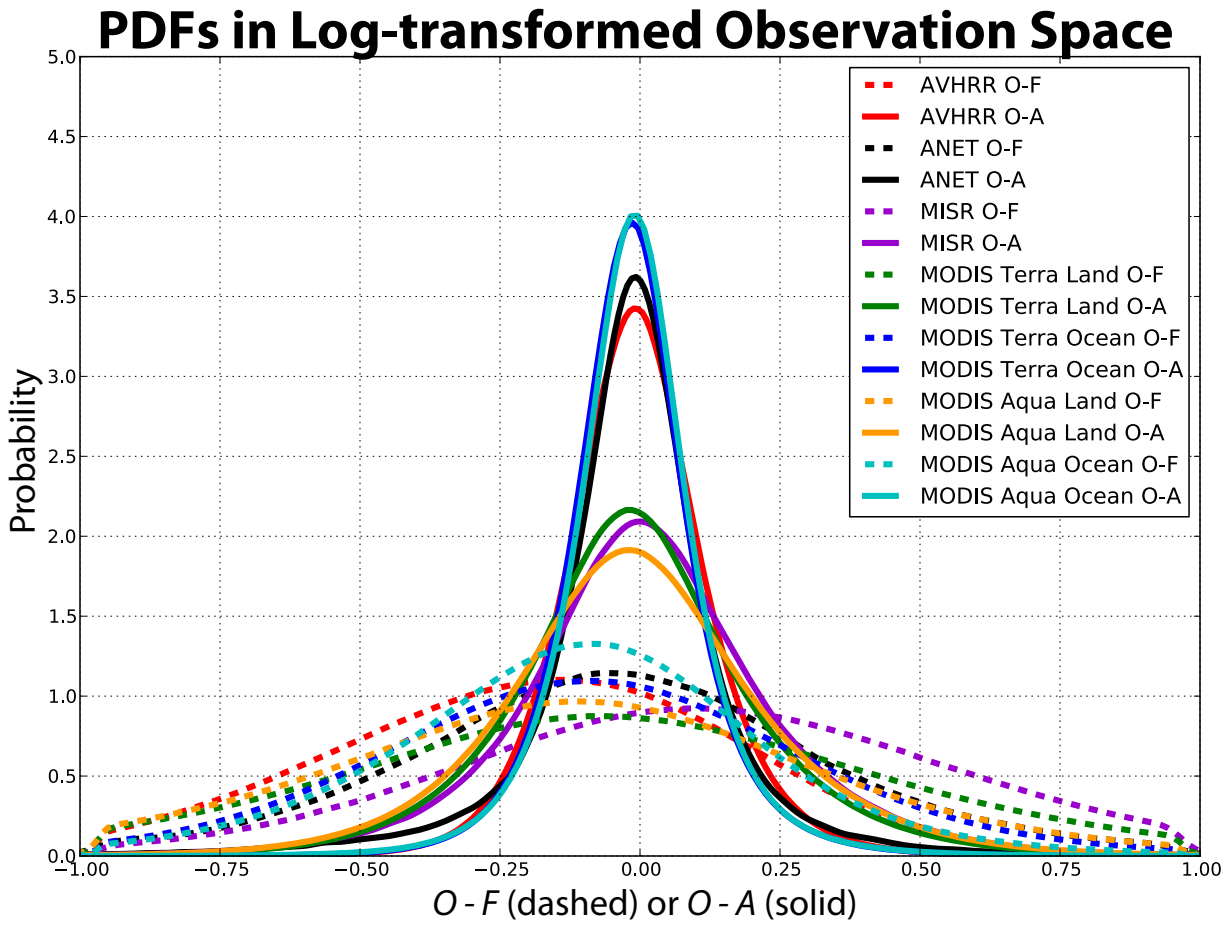

FIG. 4. Probability distribution functions (PDFs) of observation minus forecast ($O-F$; dashed) and observation minus analysis ($O-A$; solid) in observation space (co-located in space and time) for each sensor in the MERRA-2 aerosol observing system. PDFs are calculated from innovation data in log-transformed space ($ln(AOD+0.01)$) to ensure distributions are positive and Gaussian. Time periods considered are: AVHRR (1993 – 1999), MODIS Terra (2001 – 2014), MODIS Aqua (2003 – 2014), MISR (2001 – 2012), and AERONET (ANET; 2000 – 2013).

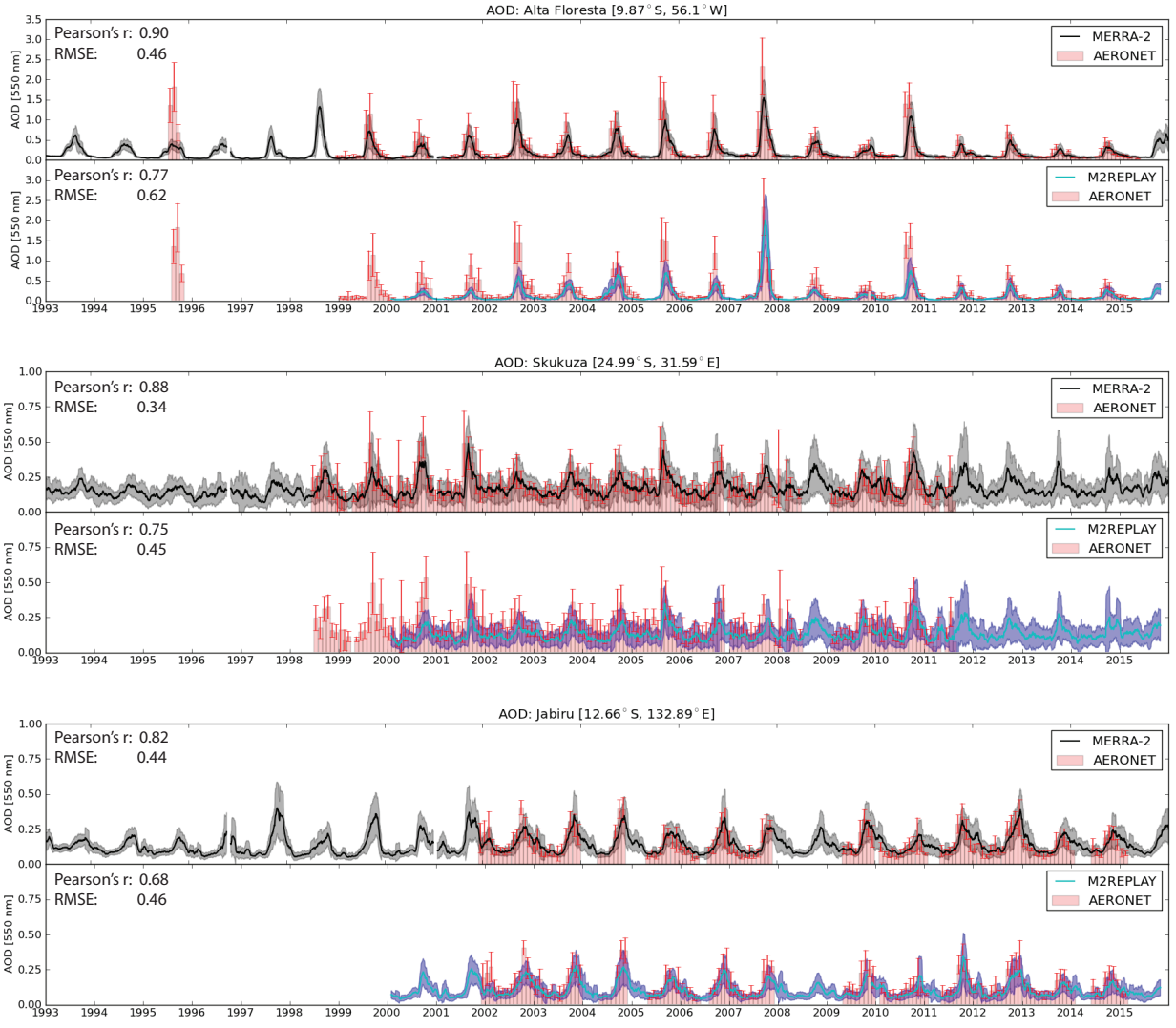

FIG. 5. Timeseries of AOD at biomass burning AERONET sites. Red bars are AERONET monthly mean AOD with error bars indicating the standard deviation of the daily observed AOD. Black and blue lines are the rolling mean AOD from MERRA-2 and the control run (M2REPLAY), respectively, with shading representing the rolling standard deviation. Correlation coefficients (r) are based on co-located hourly data for the entire timeseries shown in each panel.

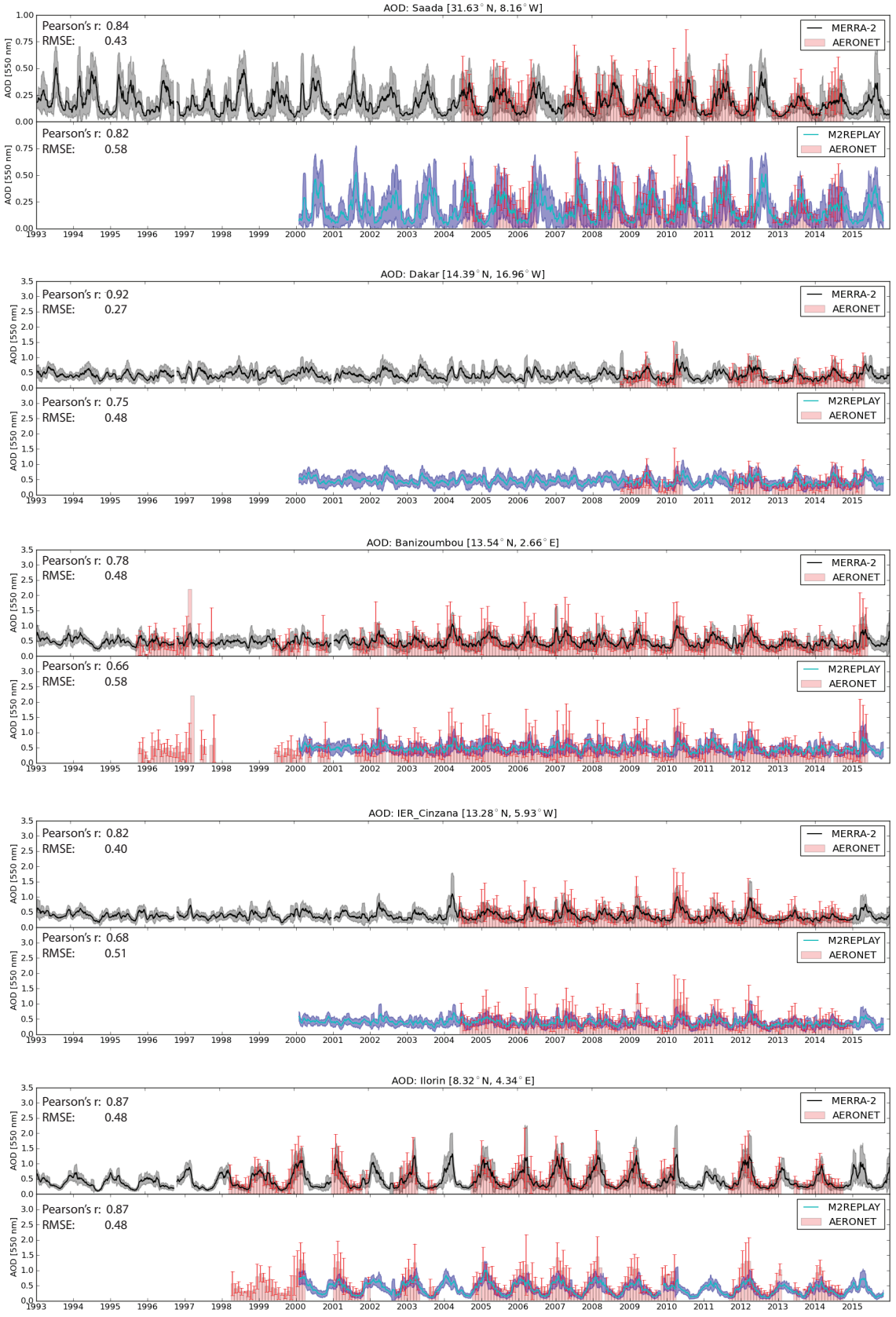

FIG. 6. Same as Fig. 5 except for sites in Northern Africa.

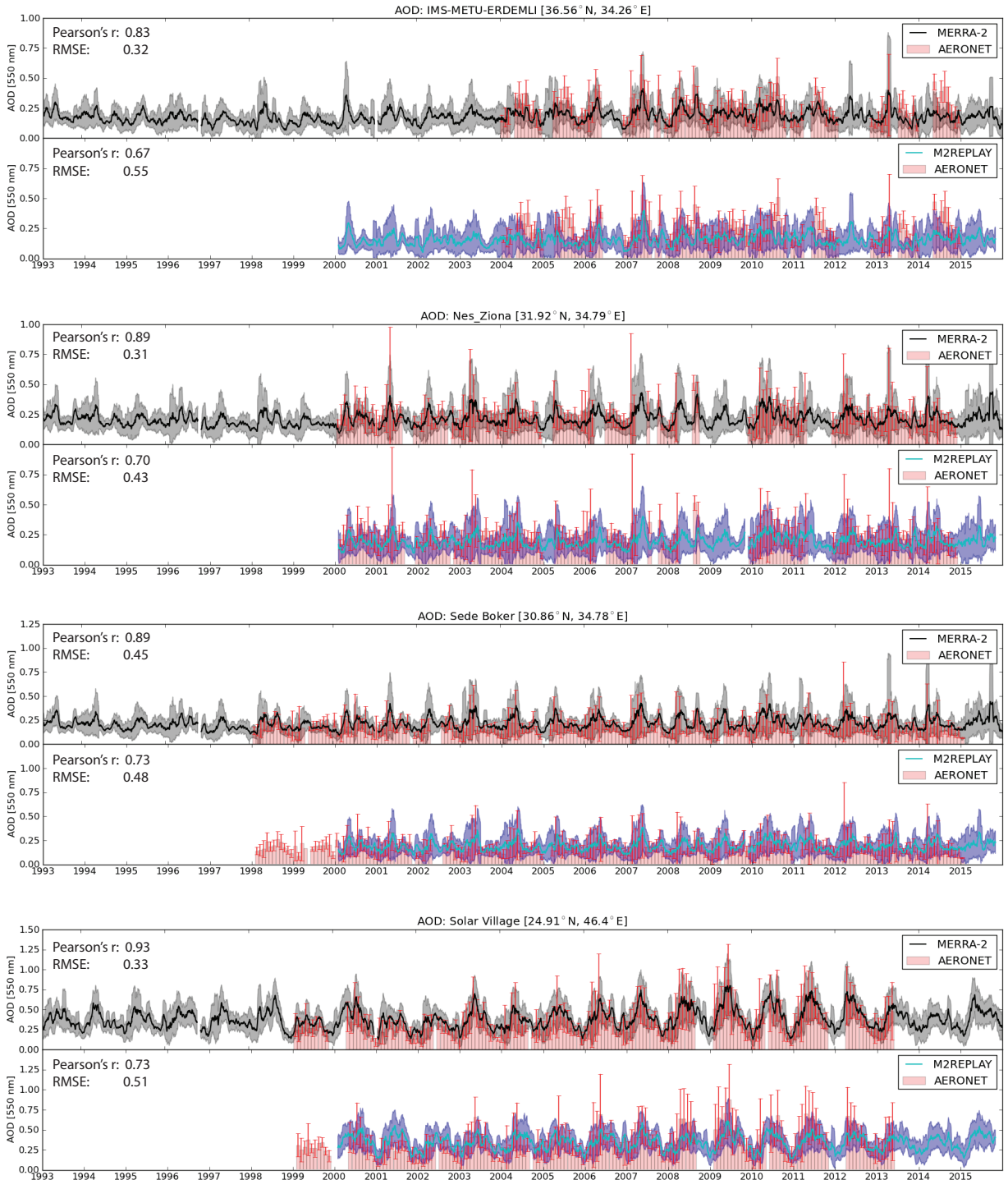

FIG. 7. Same as Fig. 5 except for sites in the Middle East.

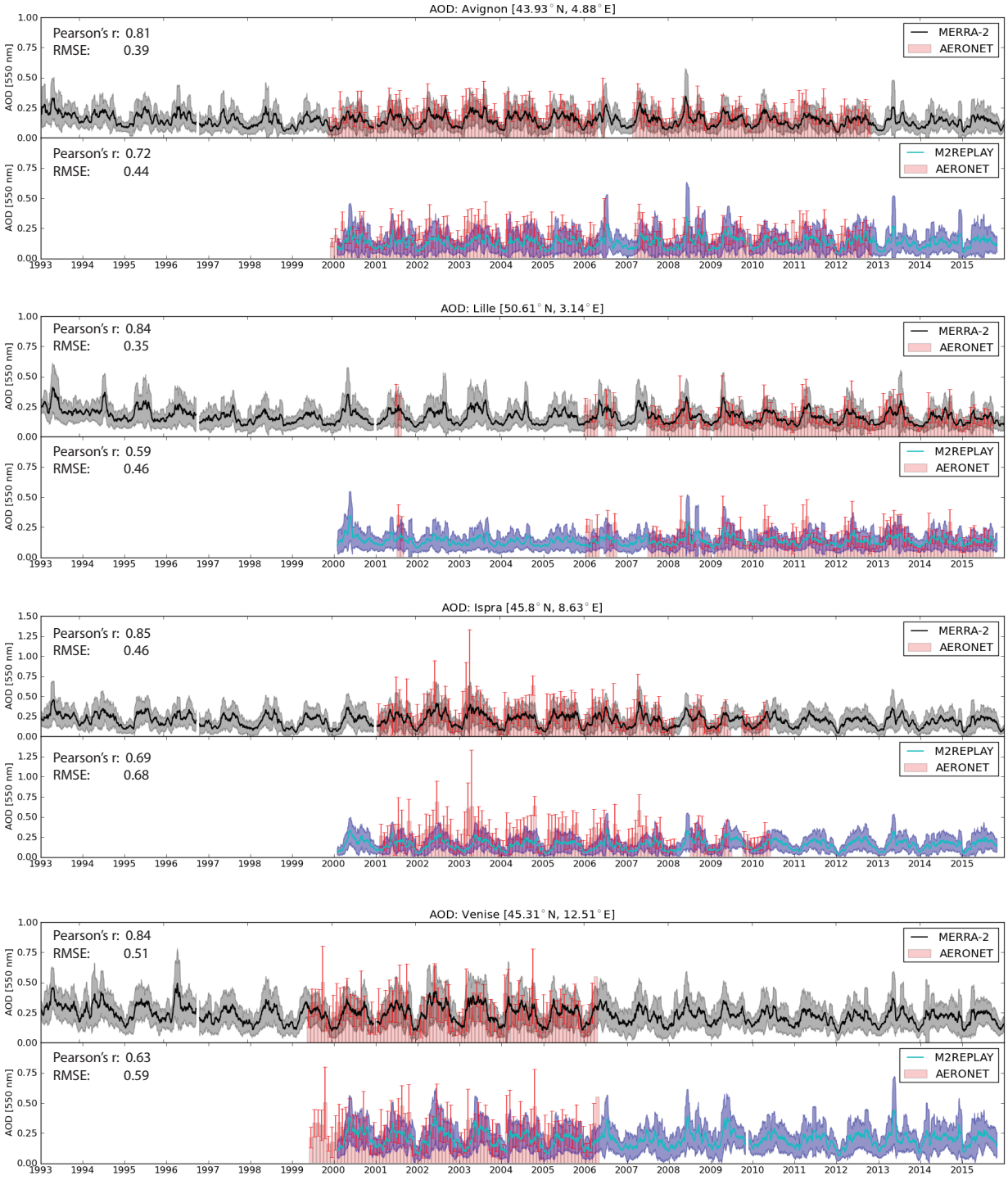

FIG. 8. Same as Fig. 5 except for sites in France and Italy.

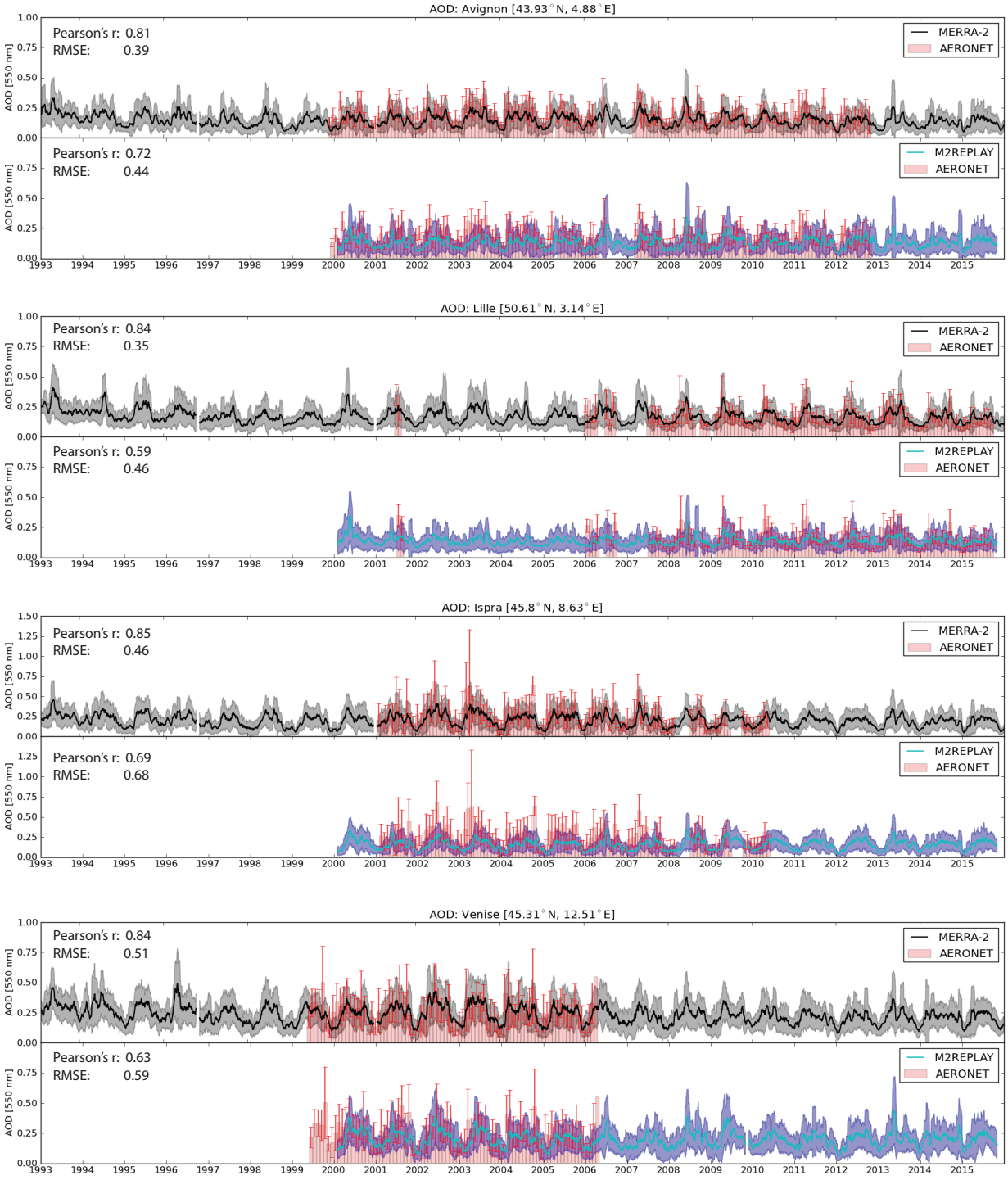

FIG. 9. Same as Fig. 5 except for other sites in Europe.

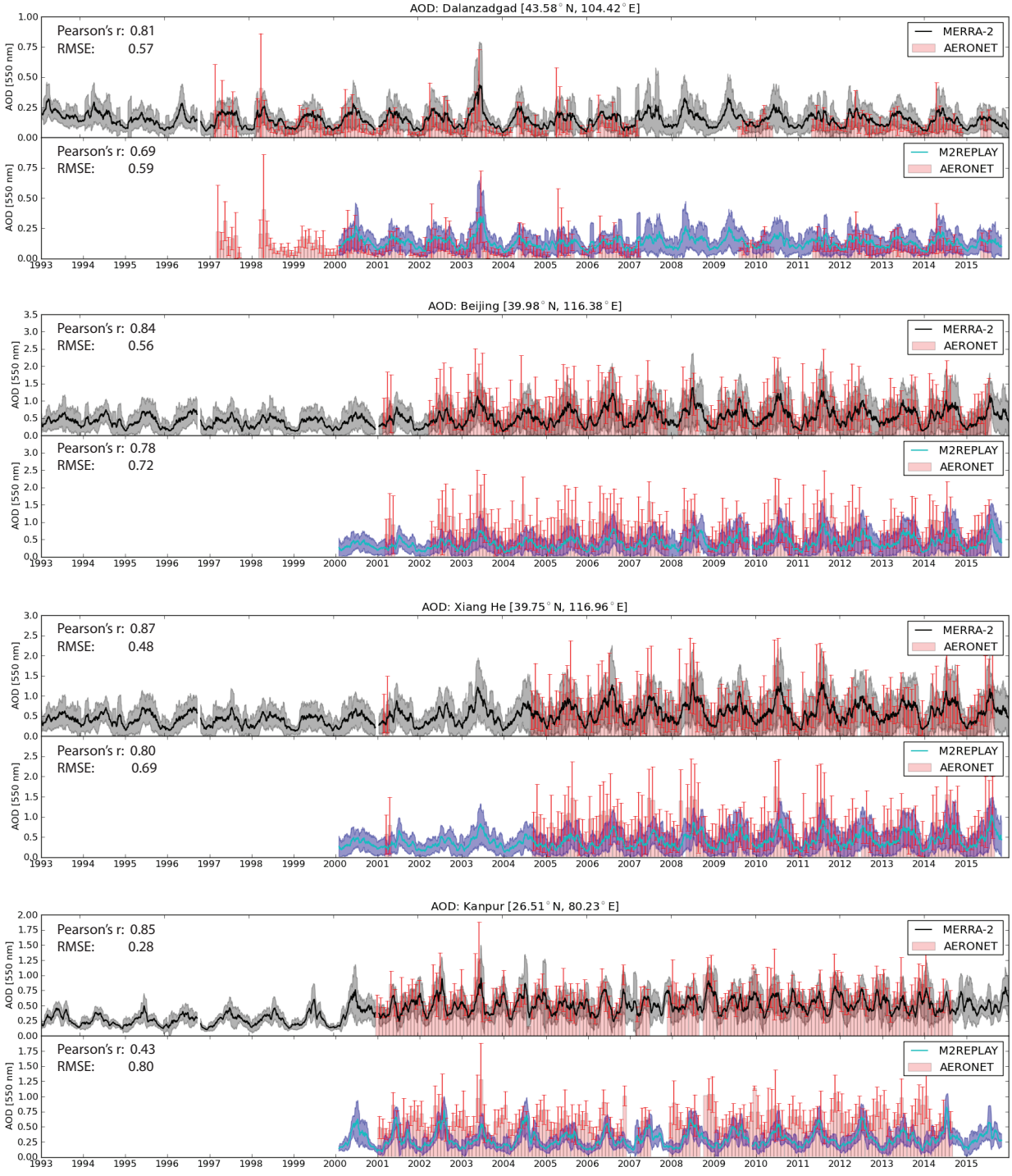

FIG. 10. Same as Fig. 5 except for South and East Asian sites.

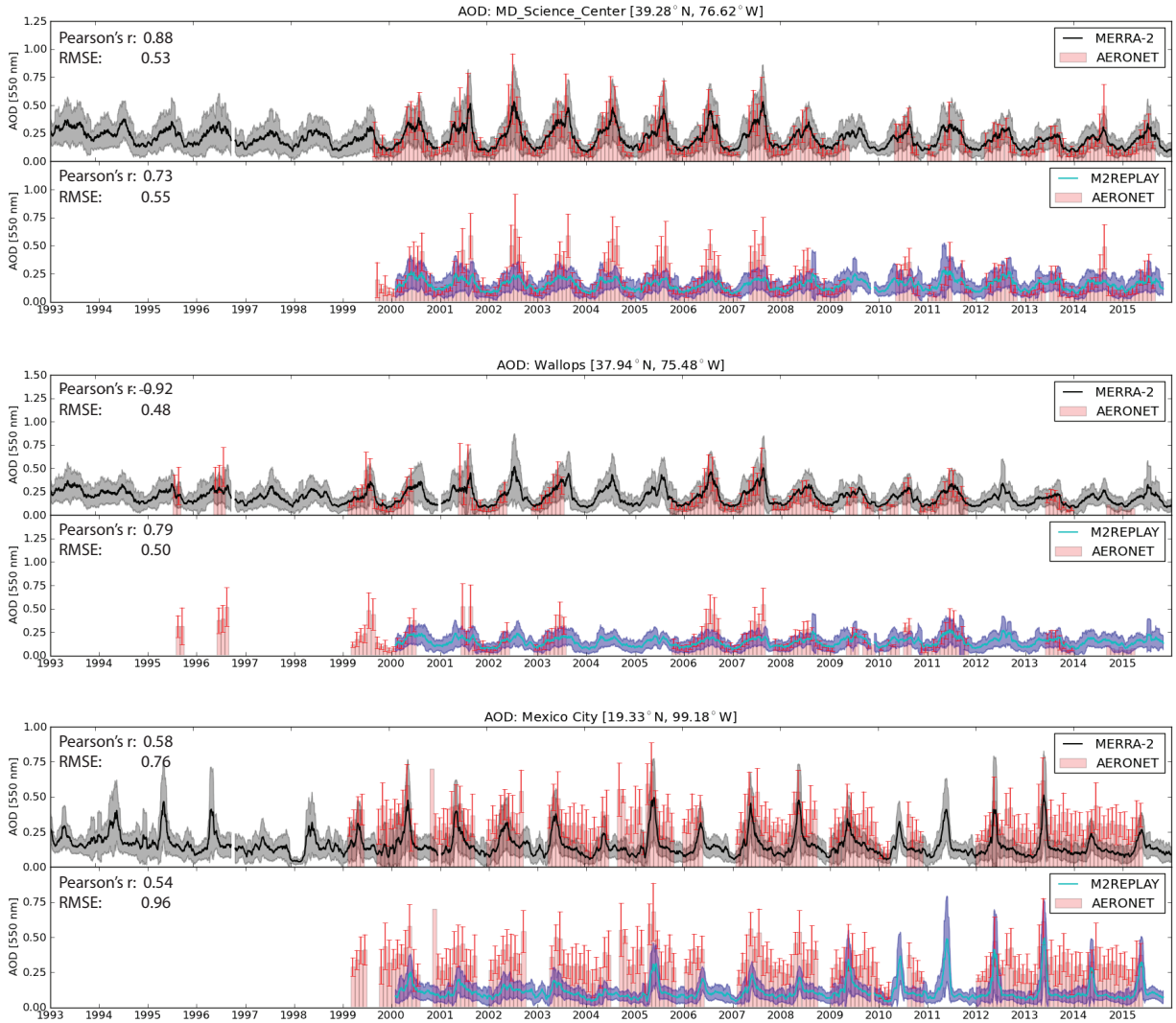

FIG. 11. Same as Fig. 5 except for polluted North American sites.

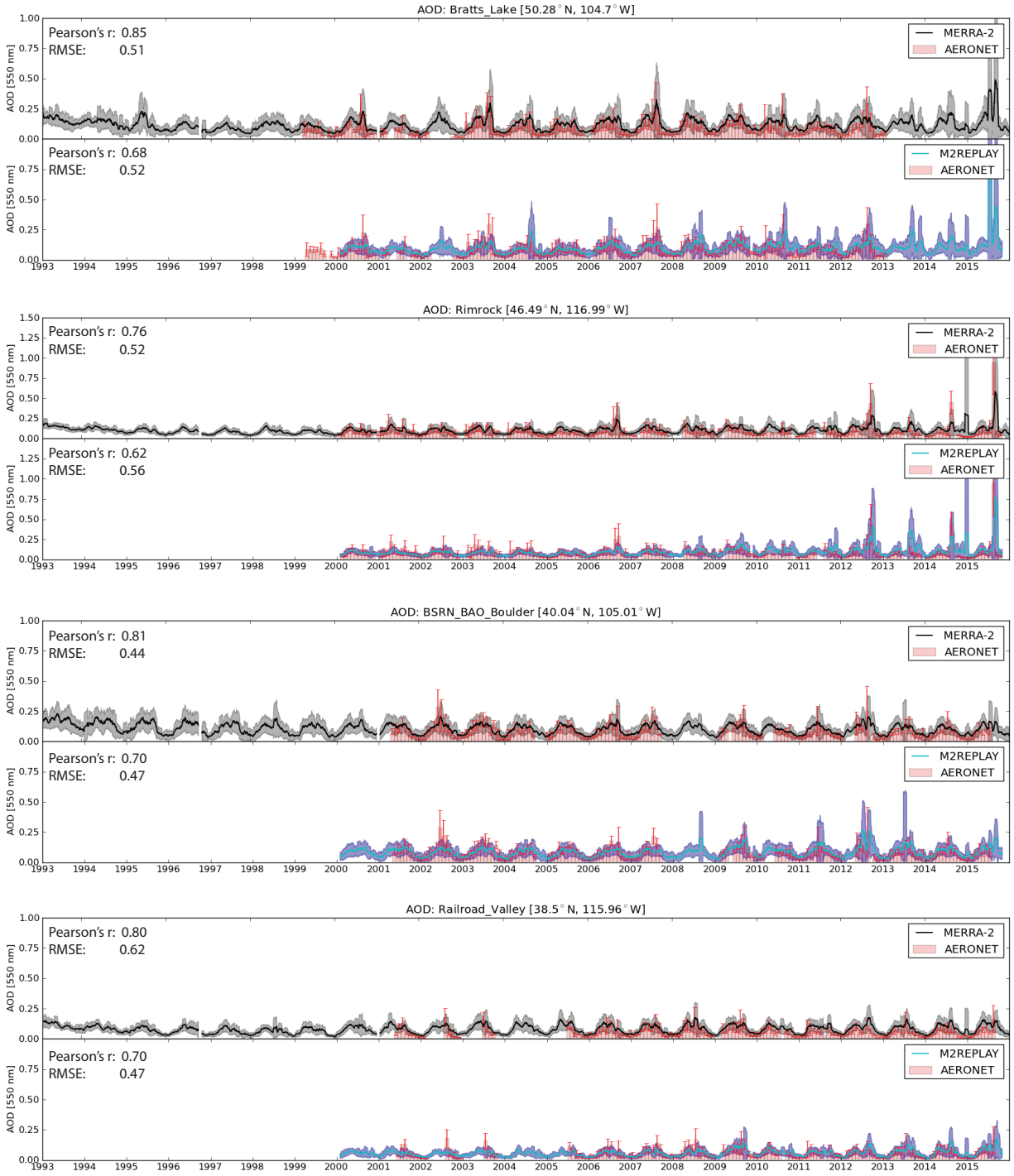

FIG. 12. Same as Fig. 5 except for sites in western North America.

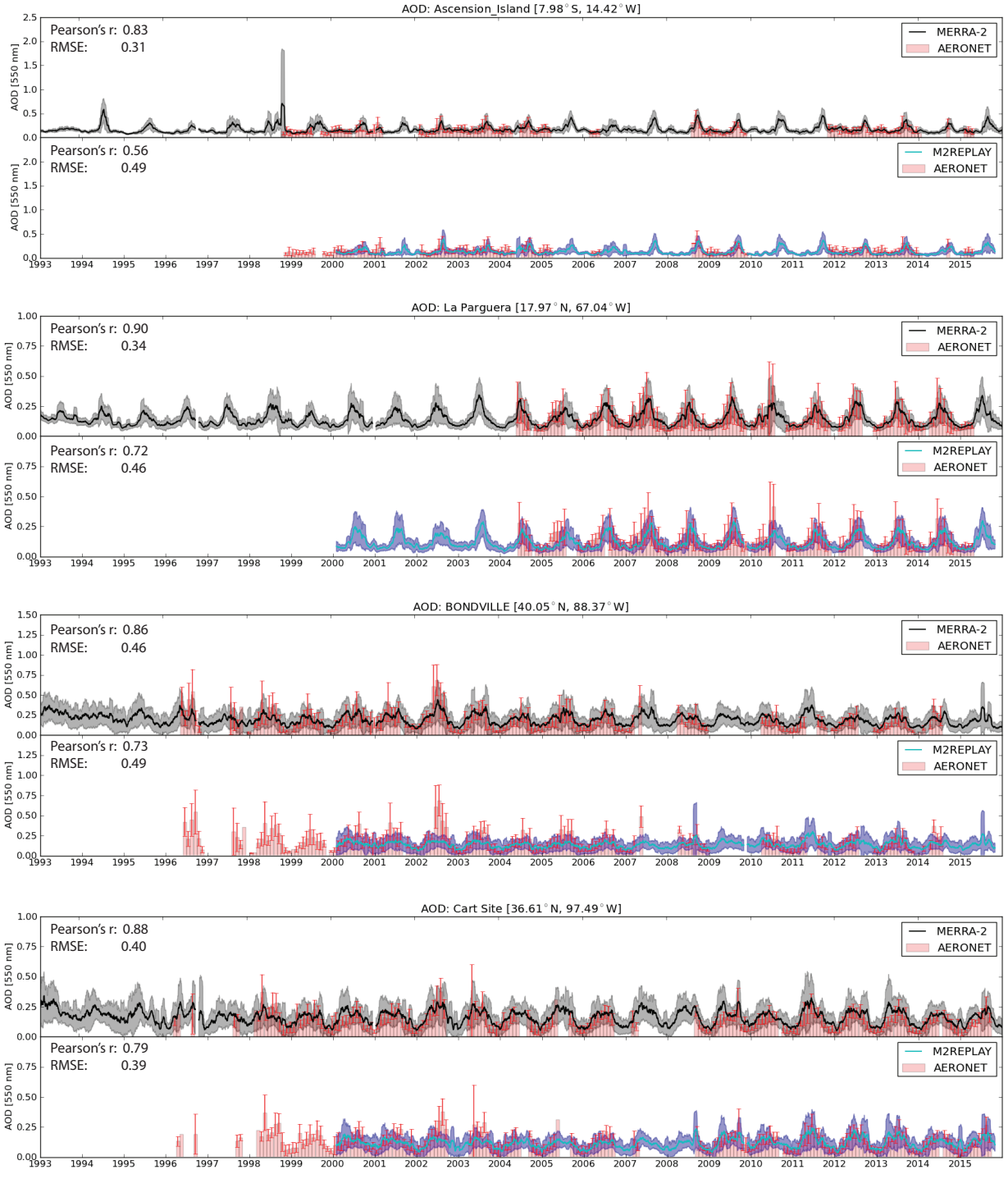

FIG. 13. Same as Fig. 5 except for clean marine and clean continental sites.